Correlation between crystal structures of CaAlSi with and without superlattice and superconducting properties

S. Kuroiwa,[1] H. Sagayama,[2] T. Kakiuchi,[3] H. Sawa,[2,3] Y. Noda,[4] and J. Akimitsu[1]
[1]*Department of Physics and Mathematics, Aoyama-Gakuin University, Sagamihara, Kanagawa 229-8558, Japan*
[2]*Photon Factory, Institute of Materials Structure Science, KEK, Tsukuba, Ibaraki 305-0801, Japan*
[3]*Department of Materials Structure Science, The Graduate University for Advanced Studies, Tsukuba, Ibaraki 305-0801, Japan*
[4]*Institute of Multidisciplinary Research for Advanced Materials, Tohoku University, Sendai 980-8577, Japan*
(Received 4 April 2006; revised manuscript received 8 June 2006; published 27 July 2006)

We have succeeded in growing a phase in CaAlSi with Al and Si atoms being distributed regularly in the AlSi layer corresponding to the B_2 plane in the AlB_2-type structure without a superlattice along the *c* axis. The field-induced magnetic response in a phase exhibits an almost isotropic characteristic for the respective crystal axis. Moreover, the $2\Delta(0)/k_BT_c$ and $\Delta C_{el}/\gamma_N T_c$ estimated by heat capacity measurements are ~3.5 and ~1.4, respectively, indicating a BCS superconductor with a weak coupling. Although CaAlSi has a two-dimensional layered structure, these results strongly suggest that the superconductivity of the phase in CaAlSi is derived from a three-dimensional electronic ground state such as a conventional *s*-wave superconductor, which is markedly different from those of superstructured CaAlSi.

DOI: 10.1103/PhysRevB.74.014517 PACS number(s): 74.70.Ad, 61.10.Nz, 74.25.Bt, 74.62.Bf

I. INTRODUCTION

The ternary silicide superconductor CaAlSi (CAS) with a layered structure belongs to a class of AlB_2-type intermetallic compounds common to MgB_2 (Ref. 1) and exhibits superconductivity with a transition temperature (T_c) of ~8 K.[2] Note that CAS has a practical advantage over MgB_2 where large single crystals are available. Therefore CAS may serve as one of the model systems for elucidating the relationship between superconducting properties and crystal structure. Because the origin of a high T_c in MgB_2 can be mainly explained by the anisotropic electronic state (two-gap/two-carrier) in honeycomb networks formed by boron atoms, for the CAS, the two-dimensional electronic ground state composed by a hybridized *sp*-orbital of Al/Si atoms has been drawing much interest as reference material for understanding the key factor leading to such a high T_c in MgB_2. Recently, Sagayama *et al.* has reported on the detailed crystal structure focusing on the AlSi layer in CAS using synchrotron x-ray and neutron diffraction analysis, which indicated the existence of a clear fivefold (5*H*-CAS) or sixfold (6*H*-CAS) superlattice along the *c*-axis caused by the distortion and rotation in the AlSi layer.[3] However, since it is extremely difficult to synthesize the single phase of polycrystalline fivefold and sixfold phases, none of them has been successful to provide detailed superconducting characteristics. Moreover, it should be noted that the so-called clean CAS (1*H*), which crystallizes to an AlB_2-like structure with *P*-6*m*2 whose Al and Si atoms are distributed regularly without a superlattice structure, is as yet unknown at this stage.

Considering the various possible types of CAS crystal structure, we should prepare a large single crystal sample and examine detailed crystal structures by synchrotron x-ray and neutron diffraction analyses. Interestingly, it turned out that our crystal exhibits no sign of clear superlattice reflection or stacking faults along the *c* axis, which is markedly different from that reported previously. Moreover, it is notable that the positions of Al and Si atoms detected by neutron diffraction are completely ordered in the *ab*-plane. We have found that our crystal has an AlB_2-like crystal structure with Al and Si atoms being distributed regularly in the B_2 plane without a superlattice structure, which turned out to be a phase (1*H*-CAS).

In this work, we report on the detailed crystal structure of 1*H*-CAS determined by synchrotron x-ray and neutron diffraction analyses and on the basic physical properties of 1*H*-, 5*H*-, and 6*H*-CAS obtained by magnetization, electrical resistivity, and heat capacity measurements. Note that the T_c of the respective phase tends to depend on a superstructured periodicity. Moreover, although the superstructured specimens (5*H*- and 6*H*-CAS) show the presence of strong anisotropy in the field-induced magnetic response and have a large superconducting gap (strong coupling), 1*H*-CAS exhibits an isotropic superconducting character for the respective crystal axis ($H\|a$ and $H\|c$,) such an ordinary BCS superconductor with *s*-wave pairing. These results strongly suggest that there is a clear correlation between superlattice structure and superconducting properties.

II. EXPERIMENTAL DETAILS AND RESULTS

The feed and seed rods were prepared by the arc melting method with a mixture of Ca (99.9%), Al (99.99%), and Si (99.999%). The single crystal of 1*H*-CAS was grown by the floating zone method under an Ar atmosphere (flow rate: 2.0 l/min). The growth rate was set to 1.5 mm/h, and the seed and feed rod were rotated in the opposite directions with a speed of 19 and 21 rpm, respectively (5*H*- and 6*H*-CAS in Refs. 2 and 4, respectively). Here, we point out that the single crystal of 1*H*-CAS can be obtained by growing the lower heating temperature than that case of superstructured specimens. The obtained ingots were confirmed to be single-crystal form and had no superlattice reflections from synchrotron x-ray Laue patterns and neutron diffraction patterns on the (00*l*) line in the reciprocal-lattice (see Fig. 1). Moreover, we performed synchrotron x-ray and neutron diffraction analyses of single-crystal 1*H*-CAS to clarify its detailed crystal structure.

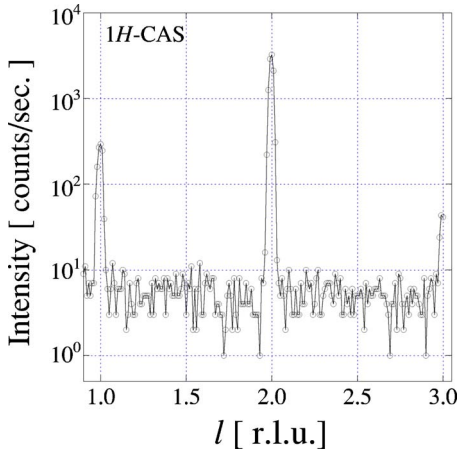

FIG. 1. (Color online) Neutron diffraction patterns on the (00*l*) line in the reciprocal-lattice for 1*H*-CAS at room temperature.

The synchrotron x-ray experiment was conducted using a conventional four-axis diffractometer installed at BL-14A at the Photon Factory, KEK, Tsukuba. The wavelength of the incident synchrotron x-ray beam monochromatized by a Si (111) double-crystal monochromator was set to 0.7505 Å, and scattered x ray was detected by an avalanche photodiode (APD).[5] The Bragg reflection intensities were measured in a full-sphere of reciprocal space in the range $2\theta < 120^{\circ}$. The total and unique number of measured reflections were 3476 and 386, respectively, and the CRYSTALSTRUCTURE program was used for refining the structural parameters. The reliability factors R and R_W were 1.1% and 1.3%, respectively, when the space group was assumed to be P-6m2 symmetry (the goodness-of-fit indicator S was 0.72). The refined structural parameters for 1*H*-CAS are listed in Table I. Here, note that it is difficult to determine the in-plane-ordered state probed by only x-ray diffraction because Al and Si are closely located in the periodic table of elements. Therefore to confirm the ordering of Al/Si atoms, we performed a precise neutron diffraction measurement because of its difference of scattering lengths for neutrons between Al/Si atoms, using a four-circle neutron diffractometer FONDER (monochromator: Ge-311, wavelength: 1.24 Å) at Japan Atomic Energy Agency (JAEA).[6] The experiment was carried out at room temperature under ambient pressure, and a single crystal of 1*H*-CAS with the dimension $2 \times 2 \times 4.5$ mm^3 was used. The intensity data obtained by neutron diffraction were corrected for absorption effect using the program DABEX. For the corrected data, a least-squares fitting analysis assuming P-6m2 symmetry was performed with the program RADIEL,[7] which yields the reliability factor $R = 2.58\%$ and $R_W = 3.06\%$, and the refined structural parameters are consistent with those determined by x-ray structure analysis. For the comparison, disordered model with $P6/mmm$ space group was applied and the result was $R = 4.37\%$ and $R_W = 5.58\%$, remarkably worse than that of the ordered model. Further, we would like to stress that the experimental values of weak intensity reflections represented by the following index: (010), (0-12), (012), (022), (120), which reflects the order parameter of Al/Si atoms, are in good agreement with those of calculation assuming the ordering state of Al/Si atoms.

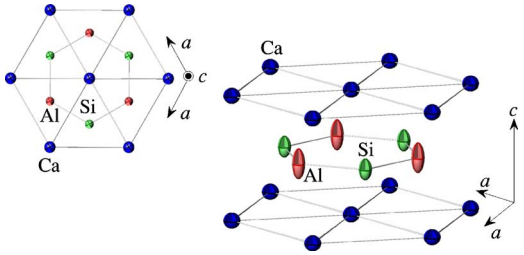

FIG. 2. (Color online) Crystal structure of 1*H*-CAS that applies an anisotropic displacement effect determined by synchrotron x-ray and neutron diffraction analyses.

Consequently, our crystal had an AlB_2-like crystal structure with Al and Si atoms being regularly distributed in the B_2 plane without a superlattice structure as shown in Fig. 2 (P-6m2 symmetry). We have also confirmed that 5*H*-CAS and 6*H*-CAS exhibit clear fivefold and sixfold superlattices along the c axis by synchrotron x-ray diffraction analysis. We investigated the magnetic response and the transport and thermal properties of 6*H*-, 5*H*- and 1*H*-CAS by dc magnetic susceptibility, electrical resistivity, and heat capacity measurements under several applied magnetic fields using a superconducting quantum interference device (SQUID) magnetometer (MPMSR2, Quantum Design Co., Ltd.) and a PPMS system (Quantum Design Co., Ltd.).

Figure 3 shows the temperature dependence of dc magnetic susceptibility at 1 mT for 6*H*-, 5*H*-, and 1*H*-CAS. The open and closed symbols denote the zero field cooling (ZFC) and field cooling (FC) processes, respectively. As shown in Fig. 3, the Meissner effect for 6*H*-, 5*H*-, and 1*H*-CAS can be observed below ~8, ~6, and ~7 K both in ZFC and FC. Inset figures show the in-plane electrical resistivity ρ_{ab} as a function of temperature at around T_c. The ρ_{ab} values of 6*H*-, 5*H*-, and 1*H*-CAS significantly decrease at T_c, as obtained from magnetization measurements. The middle critical tem-

TABLE I. Structural parameters for 1*H*-CAS with P-6m2 symmetry, where x, y, z, and occ are the atomic coordinates and occupancy, B_{eq} is the thermal parameter, and U_{nm} is the anisotropic displacement parameter. The lattice parameters a and c at room temperature are determined to be 4.196(3) Å and 4.414(4) Å, respectively.

Atom	Wyckoff letter	x	y	z	occ	B_{eq}	U_{11}	U_{22}	U_{33}	U_{12}
Ca	1a	0	0	0	1	0.918(3)	0.01211(6)	0.01211(6)	0.01062(7)	0.00601(3)
Al	1d	1/3	2/3	1/2	1	1.46(2)	0.0073(2)	0.0073(2)	0.0409(7)	0.00370(12)
Si	1f	2/3	1/3	1/2	1	0.929(11)	0.0074(2)	0.0074(2)	0.0204(4)	0.00373(11)

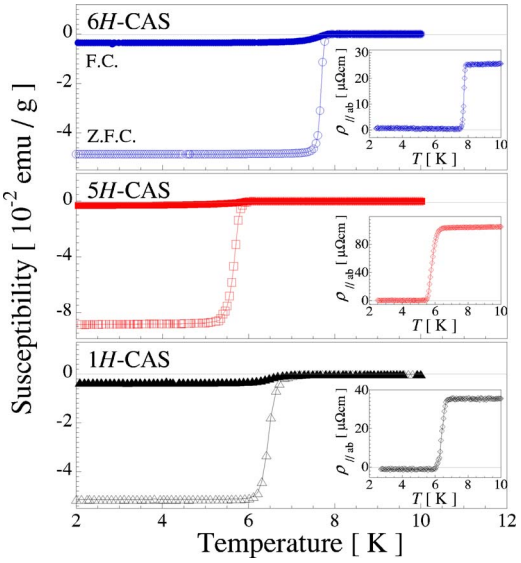

FIG. 3. (Color online) Temperature dependence of dc magnetic susceptibility at 1 mT for 6*H*-, 5*H*-, and 1*H*-CAS. Inset figures show the in-plane electrical resistivity ρ_{ab} as a function of temperature at around T_c.

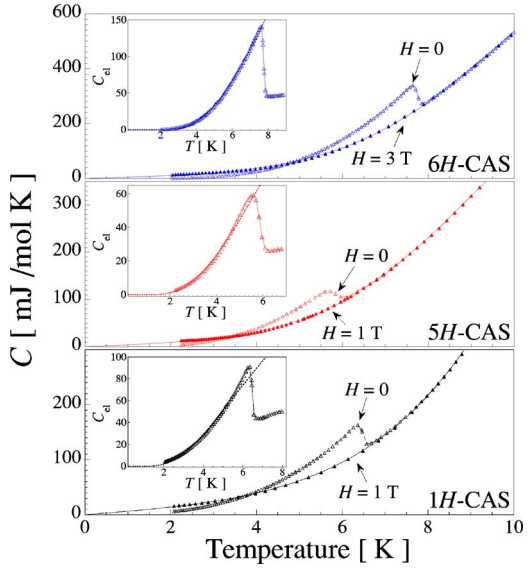

FIG. 4. (Color online) Temperature dependence of specific heat for 1*H*-CAS under zero field. The inset shows the electronic specific heat C_{el} as a function of temperature. For the solid/dotted curves, see the text.

perature $T_{c\text{-middle}}$ determined by both measurements of 6*H*-, 5*H*-, and 1*H*-CAS are ~7.75, ~5.83, and 6.45 K with transition widths of 0.2, 0.6, and 0.6 K, respectively. The ratio of interplane electrical resistivity (ρ_c) and ρ_{ab} for 1*H*-CAS is estimated to be approximately ~1.3 at room temperature, which is extremely smaller than that of superstructured specimens. Mazin *et al.* reported the electronic band structure for CAS in ordered structure with *P*-6*m*2 symmetry using the full-potential linear augmented plane-wave (FLAPW) calculations.[8] In the theoretical investigation for 1*H*-CAS, the plasma frequency for the in-plane is almost equivalent to that for the interplane, indicating that 1*H*-CAS has the isotropic effective carrier mass in the specimen. Therefore this is expected to be small resistivity anisotropy for 1*H*-CAS.

Figure 4 shows the temperature dependence of specific heat for 6*H*-, 5*H*-, and 1*H*-CAS under a zero field. The solid curves are the fitting result with $C=\gamma_N T+\beta_1 T^3+\beta_2 T^5$ where the first term is closely related to the electron part ($=C_{el}$) in the specimen, γ_N is the electronic specific heat coefficient (Sommerfeld constant), and $\beta_1 T^3+\beta_2 T^5(=C_{ph})$ is contributed by lattice vibration. By the fitting, the γ_N, which is proportional to the density of state at Fermi energy, of 6*H*-, 5*H*-, and 1*H*-CAS are estimated to be 5.07, 3.86, and 6.10 mJ/mol K^2, respectively. Moreover, the respective Debye temperatures Θ_D calculated using the formula $\beta_1=N(12/5)\pi^4 R\Theta_D^{-3}$, where β_1 is the coefficient of the T^3 term, $R=8.314$ J/mol K, and $N=3$, are listed in Table II. Inset figures show the temperature dependence of the electronic specific heat C_{el} by subtracting the phonon term C_{ph}. We clearly observed a steplike jump of C_{el} at $T_c=7.67$ K (6*H*-CAS), 5.68 K (5*H*-CAS), and 6.5 K (1*H*-CAS) corresponding to those obtained from magnetization and electrical resistivity measurements, showing evidence of bulk superconductivity. The dotted curves in the inset figures indicate the result of fitting analysis using the following equation based on a BCS theory: $C_{el}\sim\exp[-\Delta(0)/k_B T]$, where $\Delta(0)$ is the energy gap and k_B is the Boltzmann constant, for the temperature range below $T/T_c=0.8$ because of the existence of superconducting fluctuation near T_c. Because the C_{el} values of 6*H*-, 5*H*-, and 1*H*-CAS below T_c exponentially decreased with decreasing temperature, CAS has a *s*-wave symmetry, which is apparently different from the result of polycrystalline CAS obtained by previous μSR measurements.[9] Here, we point out that the upper critical field H_{c2} of 1*H*-CAS (see below) is considerably lower than that observed in the polycrystalline specimen (~2.6 T). This leads to the possibility that μSR measurement in polycrystalline specimen might have been affected by the presence of such a mixed phase as impurity. Meanwhile, $\Delta C_{el}/\gamma_N T_c$ and $2\Delta(0)/k_B T_c$, which reflect the size of the superconducting energy gap, mean the strength of electronic coupling condition; the $\Delta C_{el}/\gamma_N T_c$ and $2\Delta(0)/k_B T_c$ in the BCS weak coupling limit are ~1.43 and

TABLE II. Superconducting parameters for respective crystal axis of 6*H*-, 5*H*-, and 1*H*-CAS.

	6*H*-CAS		5*H*-CAS		1*H*-CAS	
	$H\|\|a$	$H\|\|c$	$H\|\|a$	$H\|\|c$	$H\|\|a$	$H\|\|c$
T_c [K]	7.67		5.68		6.50	
$H_{c2}(0)$ [kOe]	17.1	9.6	14.6	7.3	4.0	3.7
ξ [Å]	104	185	106	212	276	298
Γ	3.2		4.0		1.2	
Θ_D [K]	323		322		307	
γ_N[mJ/mol K^2]	5.07		3.86		6.10	
$\Delta(0)$ [meV]	1.74		1.11		0.98	
$2\Delta(0)/k_B T_c$	5.25		4.41		~3.5	
$\Delta C_{el}/\gamma_N T_c$	2.41		1.62		~1.4	

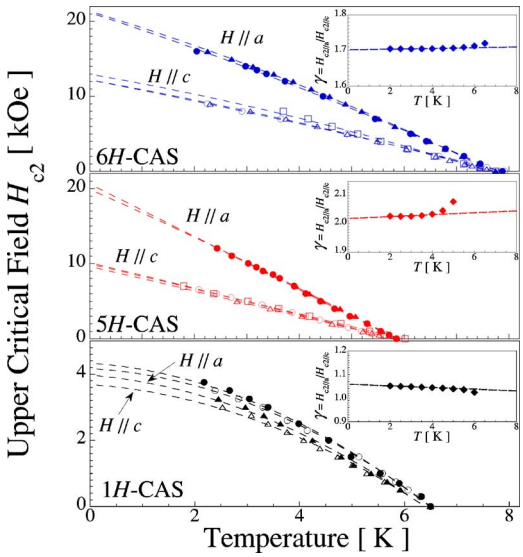

FIG. 5. (Color online) Temperature dependence of upper critical field H_{c2} for 6*H*-, 5*H*-, and 1*H*-CAS. The respective closed and open symbols indicate data measured for $H\|a$ and $H\|c$, and the circle, square, and triangle show data determined by magnetic susceptibility, electrical resistivity, and heat capacity measurements under several applied magnetic fields, respectively. The insets show the temperature dependence of the upper critical fields ratio $\gamma(=H_{c2}^{\|a}/H_{c2}^{\|c})$. These dashed lines are a visual guide.

$\sim$3.52, respectively. We estimated the $\Delta C_{el}/\gamma_N T_c$ and $2\Delta(0)/k_B T_c$ of 1*H*-CAS to be approximately $\sim$1.4 and $\sim$3.5 [$\Delta(0) \sim 0.98$ meV], respectively, suggesting that 1*H*-CAS is a conventional BCS superconductor with weak coupling. The $\Delta C_{el}/\gamma_N T_c$ and $2\Delta(0)/k_B T_c$ of 6*H*- and 5*H*-CAS are larger than those of the BCS weak coupling limit (see Table II). These results suggest that the superconductivity in superstructured specimens indicates a strong coupling regime.

Figure 5 shows the temperature dependence of upper critical field $H_{c2}^{\|i}$ ($i=c$ and a axis), which was determined from $T_{c\text{-middle}}$ obtained by the magnetic susceptibility, electrical resistivity, and specific heat at respective magnetic fields (inset shows the upper critical field ratio γ vs temperature), and these dashed lines are a visual guide. For 6*H*- and 5*H*-CAS, the field-induced magnetic response between the in-plane and the interplane has a strong anisotropy probably due to the two-dimensional electronic state derived from a layered structure. It is notable, however, that the $H_{c2}^{\|a}$ and $H_{c2}^{\|c}$ of 1*H*-CAS show similar temperature dependences, suggesting that 1*H*-CAS has an extremely small anisotropy of magnetic response due to the three-dimensional electronic ground state. According to the theoretical investigation, Mazin *et al.* also theoretically suggested that the Fermi level of 1*H*-CAS was mainly formed by only one band of Ca $d_{3z^2-r^2}$ orbital, and thereby has extremely three-dimensional characteristics.[8] Meanwhile, the anisotropy of magnetic response in superstructured specimens can be possibly described by the substantial change of electronic ground state due to the variation of Al-Si bonding from a hybridized sp^2- to sp^3-orbital because of the buckling of the AlSi layers. For these three phases, we have estimated $H_{c2}^{\|i}(0)$ using the Werthamer-Herfand-Hohenberg (WHH) equation, $H_{c2}(0) = 0.69(-dH_{c2}/dT)T_c$, for the type II superconductor in a dirty limit.[10,11] Moreover, the anisotropic parameter Γ was determined using the anisotropic Ginzburg-Landau (GL) formula

$$\sqrt{\Gamma} = \sqrt{\frac{m_c}{m_a}} = \frac{H_{c2}^{\|a}}{H_{c2}^{\|c}} = \frac{\xi_a}{\xi_c}, \tag{1}$$

where m_i and ξ_i are the effective mass and GL-coherence length. We calculated the ξ_i using $H_{c2}^{\|a} = \Phi_0/(2\pi\xi_a\xi_c)$ and $H_{c2}^{\|c} = \Phi_0/(2\pi\xi_a^2)$ where Φ_0 is the quantum flux. The estimated $H_{c2}^{\|i}(0)$ and ξ_i for the respective crystal axis and anisotropic parameter Γ are listed in Table II. Note that the absolute value of $H_{c2}^{\|i}(0)$ and anisotropic parameter Γ ($\sim$1.2) of 1*H*-CAS are much smaller than those of the superstructured specimens. It is theoretically known that H_{c2} determined by the formula $H_{c2} \sim \Phi_0/\pi\xi_0 l \sim 3ckT_c/ev_F l$, where ξ_0 is the BCS coherence length, l is the mean free path, and v_F is the Fermi velocity, derived from the BCS theory; $\xi_0 = hv_F/2\pi^2\Delta(0)$. Therefore the smaller $H_{c2}^{\|i}(0)$ of 1*H*-CAS in comparison with that of the superstructured specimens is closely related to the size of the energy gap, which yields $\Delta(0)_{1H} \sim 0.98$ meV and $\Delta(0)_{6H} \sim 1.74$ meV, as obtained by heat capacity measurement. In addition, the similar T_c in the respective phases implies that the mean free path in superstructured specimens is suppressed in comparison with that in 1*H*-CAS because of the superstructure due to the rugged AlSi layer.

III. SUMMARY

We have succeeded in growing the superstructured specimens (6*H*- and 5*H*-CAS) and their phase (1*H*-CAS) with the in-plane ordered state without a superlattice along the *c*-axis. We examined their physical properties in detail by magnetization, electrical resistivity, and heat capacity measurements. The obtained superconducting parameters of 6*H*-, 5*H*-, and 1*H*-CAS are listed in Table II. Note that the superconductivity of 1*H*-CAS can be well-described by a conventional BCS superconductor in a weak coupling regime; it had a typical thermal property [$\Delta C_{el}/\gamma_N T_c \sim 1.4$ and $2\Delta(0)/k_B T_c \sim 3.5$] and an isotropic magnetic response probably due to the three-dimensional electronic state. On the other hand, the size of the superconducting gap (strong coupling regime), $H_{c2}^{\|i}(0)$, and anisotropic parameter Γ in 6*H*- and 5*H*-CAS are extremely larger than those in 1*H*-CAS. These results suggest that the electronic ground state in superstructured specimens is significantly changed from three-dimensionality for 1*H*-CAS to two-dimensionality which reflects the crystal structure. The origin of the difference between superstructured specimens and 1*H*-CAS remains to be clarified.

ACKNOWLEDGMENTS

This work was partly supported by the 21st COE program, "High-Tech Research Center" Project for Private Universities: matching fund subsidy from MEXT (Ministry of Education, Culture, Sports, Science and Technology; 2002–2004).

[1] J. Nagamatsu, N. Nakagawa, T. Muranaka, Y. Zenitani, and J. Akimitsu, Nature (London) **410**, 63 (2001).
[2] M. Imai, E. I-Hadi, S. Sadki, H. Abe, K. Nishida, T. Kimura, T. Sato, K. Hirata, and H. Kitazawa, Phys. Rev. B **68**, 064512 (2003).
[3] H. Sagayama, Y. Wakabayashi, H. Sawa, T. Kamiyama, A. Hoshikawa, S. Harjo, K. Uozato, A. K. Ghosh, M. Tokunaga, and T. Tamegai, J. Phys. Soc. Jpn. **75**, 043713 (2006).
[4] A. K. Ghosh, M. Tokunaga, and T. Tamegai, Phys. Rev. B **68**, 054507 (2003).
[5] S. Kishimoto, N. Ishizawa, and T. P. Vaalsta, Rev. Sci. Instrum. **68**, 384 (1998).
[6] Y. Noda, H. Kimura, R. Kiyanagi, A. Kojima, Y. Morii, N. Minakawa, and N. Takesue, J. Phys. Soc. Jpn. **70**, A456 (2001).
[7] P. Coppens, T. N. Guru, P. Leung, E. D. Stevens, P. J. Becker, and Y. W. Yang, Acta Crystallogr., Sect. A: Cryst. Phys., Diffr., Theor. Gen. Crystallogr. **35**, 63 (1979).
[8] I. I. Mazin and D. A. Papaconstantopoulos, Phys. Rev. B **69**, 180512(R) (2004).
[9] S. Kuroiwa, H. Takagiwa, M. Yamazawa, J. Akimitsu, K. Ohishi, A. Koda, W. Higemoto, and R. Kadono, J. Phys. Soc. Jpn. **73**, 2631 (2004).
[10] E. Helfand and N. R. Werthamer, Phys. Rev. **147**, 288 (1966).
[11] K. Maki, Phys. Rev. **148**, 362 (1966).